Neuropharmacology 79 (2014) 515–524

Contents lists available at ScienceDirect

Neuropharmacology

journal homepage: www.elsevier.com/locate/neuropharm

Characterization of altered intrinsic excitability in hippocampal CA1 pyramidal cells of the Aβ-overproducing PDAPP mouse

T.L. Kerrigan [a], J.T. Brown [a, b], A.D. Randall [a, b, *]

[a] School of Physiology and Pharmacology, University of Bristol, University Walk, Bristol BS8 1TD, UK
[b] Institute of Biomedical and Clinical Sciences, University of Exeter Medical School, The Hatherly Building, Exeter EX4 4PS, UK

ARTICLE INFO

Article history:
Received 30 April 2013
Received in revised form
21 August 2013
Accepted 4 September 2013

Keywords:
Alzheimer's disease
Hippocampus
Electrophysiology
Excitability
Brain slice
Action potential

ABSTRACT

Transgenic mice that accumulate Aβ peptides in the CNS are commonly used to interrogate functional consequences of Alzheimer's disease-associated amyloidopathy. In addition to changes to synaptic function, there is also growing evidence that changes to intrinsic excitability of neurones can arise in these models of amyloidopathy. Furthermore, some of these alterations to intrinsic properties may occur relatively early within the age-related progression of experimental amyloidopathy. Here we report a detailed comparison between the intrinsic excitability properties of hippocampal CA1 pyramidal neurones in wild-type (WT) and PDAPP mice. The latter is a well-established model of Aβ accumulation which expresses human APP harbouring the Indiana (V717F) mutation. At the age employed in this study (9–10 months) CNS Abeta was elevated in PDAPP mice but significant plaque pathology was absent. PDAPP mice exhibited no differences in subthreshold intrinsic properties including resting potential, input resistance, membrane time constant and sag. When CA1 cells of PDAPP mice were given depolarizing stimuli of various amplitudes they initially fired at a higher frequency than WT cells. Commensurate with this, PDAPP cells exhibited a larger fast afterdepolarizing potential. PDAPP mice had narrower spikes but action potential threshold, rate of rise and peak were not different. Thus not all changes seen in our previous studies of amyloidopathy models were present in PDAPP mice; however, narrower spikes, larger ADPs and the propensity to fire at higher frequencies were consistent with our prior work and thus may represent robust, cross-model, indices of amyloidopathy.

This article is part of a Special Issue entitled 'Neurodevelopment Disorder'.

1. Introduction

Excessive generation and/or accumulation of beta-amyloid peptides are produced through enzymatic cleavage of amyloid precursor protein (APP) via the sequential activity of beta and gamma secretases, respectively (Zhang et al., 2012). The centre-stage position of the amyloid hypothesis in the pathobiology of AD has motivated the generation of a considerable number of transgenic mouse lines which in CNS Aβ levels become hugely elevated in an age-dependent manner. These mice have become widely-employed experimental models of AD-associated progres-

2012; Morrissette et al., 2009).

A plethora of neurophysiological studies of transgenic mice with elevated Aβ have appeared in the published literature over the last 15 years (Randall et al., 2010). Like the very first papers, many of these have focussed on analysis of synaptic function and plasticity in hippocampus (Brown et al., 2005; Chapman et al., 1999; Fitzjohn et al., 2008; Hsia et al., 1999; Larson et al., 1999; Oddo et al., 2003), or cerebral cortex (Roder et al., 2003). More recently other aspects of neurophysiological function in Aβ overproducing mice have begun to receive increased attention, in particular significant alterations to intrinsic excitability of single neurones (Brown et al., 2011; Driver et al., 2007; Minkeviciene et al., 2009; Verret et al., 2012; Wykes et al., 2012) and disturbances to synchronized

* Corresponding author. School of Physiology and Pharmacology, University of Bristol, University Walk, Bristol BS8 1TD, UK. Tel.: +44 (0)117 3311931.
E-mail address: A.D.Randall@bristol.ac.uk (A.D. Randall).

0028-3908
http://dx.doi.org/10.1016/j.neuropharm.2013.09.004

activity in defined neuronal networks (Brown et al., 2011; Driver et al., 2007; Palop et al., 2007; Verret et al., 2012).

At the single cell level, some studies have reported little or no change to the intrinsic excitability of hippocampal or cortical neurones in the face of a significant amyloid load (Rocher et al., 2008; Spencer et al., 2006). More recent studies, however, have pointed to various modifications to intrinsic excitability properties in Aβ overproducing mice; these include depolarized resting potentials and consequent hyperexcitability in Layer II/III cortical pyramidal cells of APdE9 double transgenic mice (Minkeviciene et al., 2009) and depression of the slow after-hyperpolarization (sAHP) of hippocampal CA1 pyramidal cells of TAS10 mice (Driver et al., 2007). Changes have also been reported in inhibitory cells, for example the resting potential of parvalbumin-positive, fast spiking, GABAergic interneurones of layer II/III of the parietal cortex of J20 mice was reported to be depolarized by ~6 mV, furthermore spike amplitude was decreased compared to controls – whereas neither change was seen in pyramidal cells of the same brain area (Verret et al., 2012).

In our own laboratory, studies of the Aβ-overproducing PSAPP double transgenic mouse line revealed an intrinsic hyperexcitability in CA1 pyramidal cells (CA1-PC) at approx 8 months of age. This was manifest as an increased burstiness in the pattern of action potential firing triggered by weakly suprathreshold 500 ms depolarizing current injections (Brown et al., 2011). This intrinsic hyperexcitability was parallelled by an enhanced after-depolarizing potential (ADP) and changes to action potential waveform including, a reduced spike width and a reduction in spike height and rate of rise which likely result from a ~50% loss of functional voltage-gated Na^+ channels revealed by voltage clamp recordings from nucleated macropatches (Brown et al., 2011), a change that we demonstrated also occurs in another Aβ overproducing mouse, Tg2576 (Brown et al., 2011). Changes to action potential properties, and the Ca^{2+} entry they evoke, was also seen in CA1 pyramidal cells of preplaque CRND8 mice (Wykes et al., 2012), in line with our work (Brown et al., 2011), this group found spikes to be narrower and suggested this may arise from increased levels of Kv3.1 channels.

Thus, studies at the single cell level in a range of different Aβ-overproducing mice have uncovered a number of changes to intrinsic excitability properties in various cortical and hippocampal cell-types in various different models. However, because almost every study considers a different model and/or cell type (and usually involves what can be significant methodological differences) what remains unclear is which, if any, of these changes are consistently and robustly observed across multiple Aβ-overproducing mouse models. As a starting point to addressing this question we have performed a new study of the intrinsic properties of CA1-PC under conditions close to identical to those we employed previously (Brown et al., 2011), but rather than studying the PSAPP mouse we employed an alternative Aβ-overproducing transgenic line, namely PDAPP (Games et al., 1995). This mouse transgenically expresses APP harbouring the Indiana mutation (which lies at the gamma secretase site) rather than the Swedish mutation, which lies at the beta secretase site of APP, and which is combined with the presenilin 1 M146L mutation in PSAPP mice (McGowan et al., 1999). Our experiments point to both similarities and differences from the changes observed in PSAPP mice, and may start to highlight neurophysiological changes that occur in multiple Aβ overproducing lines.

2. Methods

2.1. Transgenic mice

Male PDAPP transgenic mice and WT littermate controls (Games et al., 1995) were the subjects of this study. This single transgenic mouse line expresses human APP carrying the Indiana (V717F) mutation. Transgene expression is directed by the PDGF-β chain promoter and results in an age-dependent accumulation of Aβ peptides including the production of amyloid plaques in older animals (Games et al., 1995). All studies where performed on mice aged 9–10 months and were designed to compare the phenotype of PDAPP mice with WT littermates. In our cohorts at this age there is no significant amyloid plaque pathology but elevated levels of Aβ peptides were confirmed in PDAPP mice using Western blotting (see below). All animals were supplied by Eli Lilly as part of the Pharmacog initiative. The animals arrived just prior to the study age and arrived in three separate shipments over an 8 month period. In total over 30 mice of each genotype contributed to this study. From weaning onwards mice were singly housed with access to food and water ad libitum. They experienced a standard 12:12 light/dark cycle. All procedures were carried out in accordance with local ethical guidelines and UK Home Office legislation set out in the Animals (Scientific Procedures) Act (1986).

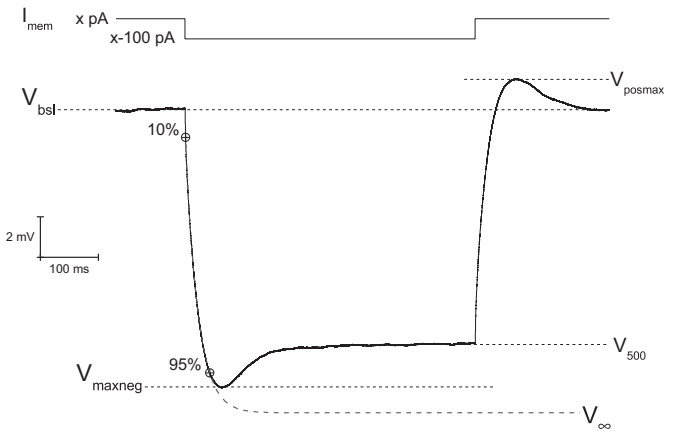

Fig. 1. Schematic illustration of methods used to measure passive intrinsic properties of CA1 pyramidal cells. Passive properties were determined from the voltage response to a negative current injection applied to cells with a baseline voltage (V_{bsl}) set to ~−82 mV with a suitable level of current injection (x). The cell is hyperpolarized by injecting 100 pA of negative current for 500 ms (such that the current passing at that time is x − 100 pA). When this occurs the membrane potential charges towards a negative peak (V_{maxneg}) over a period of around 15–50 ms. Following this the membrane potential "sags" back in a depolarized direction reaching a steady state level (V_{500}) before the end of the current injection. When the negative current step is ceased and returned to the resting level of x pA the membrane potential transiently overshoots to a peak (V_{posmax}) before returning to V_{bsl}. As well as measuring the voltage levels described above we fit a single exponential decay between the 10 and 95% time points of the initial charging response (crossed circles). From this fit we extract membrane time constant (τ_{mem}) and also the extrapolated voltage at infinite time (V_∞).

2.2. In vitro electrophysiological recordings

Mice were sacrificed by cervical dislocation. Brains were rapidly removed and placed in ice cold (~4 °C), sucrose-based cutting solution comprising (in mM): sucrose, 189; D-glucose, 10; $NaHCO_3$, 26; KCl, 3; $MgCl_2$, 5; $CaCl_2$, 0.1; NaH_2PO_4, 1.25, continuously bubbled with carbogen (95% O_2, 5% CO_2). The whole brain (minus the cerebellum) was mounted on a steel plate and 300 μm horizontal sections were cut using a vibratome (Leica VT1200). After sectioning, hippocampal slices were transferred to a submerged storage chamber containing artificial cerebrospinal fluid (aCSF) comprising (in mM): NaCl, 124; KCl, 3; $NaHCO_3$, 26; $CaCl_2$, 2; NaH_2PO_4, 1.25; $MgSO_4$, 1; D-glucose, 10 and equilibrated with 95% O_2 and 5% CO_2 and were gradually heated to ~32–34 °C for 30 min, after which they were stored at room temperature. Slices were transferred to a submersion-style recording chamber that was continuously perfused (1–2 ml min^{-1}) with aCSF. The aCSF temperature was maintained at 33 ± 1 °C by a feedback circuit. Pyramidal neurones were visually identified within *s. pyramidale* of area CA1 using infra-red differential interference contrast optics. Whole cell current recordings were made using fire-polished, borosilicate glass microelectrodes (3–5 MΩ). The pipette solution contained (mM): K-gluconate, 145; NaCl, 20; K-HEPES, 10; EGTA, 0.2; Na-GTP, 0.3; Mg-ATP, 4; pH 7.3, 285–290 mOsm. A liquid junction potential error (−15 mV) between this solution and the aCSF was corrected for arithmetically.

All recordings were made using a MultiClamp 700B amplifier (Molecular Devices, Union City, CA). Recordings were lowpass filtered (10 kHz) and then digitized (100 kHz) using a Digidata 1440A and stored on a personal computer using pClamp10 electrophysiology software.

2.3. In vitro electrophysiology data analysis

Analysis of current clamp recordings, including action potential waveform analysis was carried out with custom written routines within the Matlab

environment. Resting potential was defined as the average zero current potential measured in current clamp over a 10 s period soon after gaining whole cell access – it was always the first measurement made in every cell, because we have found that some protocols which drive repeated action potential firing can cause long term changes to resting potential (in essence a form of activity-dependent persistent intrinsic plasticity). Other subthreshold membrane properties, namely input resistance, membrane time constant and "sag" were determined from the voltage responses to 500 ms duration, −100 pA current injections. Fig. 1 illustrated the various voltage levels and the fit used to perform these various measurements. The membrane time constant (τ_{mem}) was determined by fitting a best single exponential decay to the negative-going membrane charging trajectory produced by current injection. This fit was made between timepoints corresponding to voltages 10% and 95% of the distance between the pre-stimulus baseline (V_{bsl}) and the peak hyperpolarization achieved during the current injection (V_{maxneg}). Input resistance was determined in two different ways, both based upon Ohm's law. The first measure (R_i) used the voltage difference between the pre-stimulus membrane potential (V_{bsl}, ~−82 mV) and the mean steady state voltage observed in the final 10 ms of the 500 ms of current injection (V_{500})-

$$R_i = 100/(V_{bsl} - V_{500})$$

this measurement therefore incorporates the decrease in membrane resistance that occurs as the result of activation of HCN channels and the voltage "sag" this elicits. Our second measure of membrane resistance (R_{xtr}) instead employs the voltage difference between V_{bsl} and the infinite time asymptote of the exponential fit to the membrane charging curve (V_∞).

$$R_{xtp} = 100/(V_{bsl} - V_\infty)$$

Similarly, two measures of "sag" were made. The first (Sag_{sub}) used the voltage difference between the peak hyperpolarization (V_{maxneg}) observed during the current stimulus and V_{500}; with sag being defined as

$$Sag_{sub} = 100*(V_{maxneg} - V_{500})/(V_{maxneg} - V_{bsl}).$$

The alternative measure of sag (Sag_{fit}) employed the value of V_∞ in place of V_{maxneg}

$$Sag_{fit} = 100*(V_\infty - V_{500})/(V_\infty - V_{bsl}).$$

Due to the effects of sag activation reducing the peak hyperpolarization achieved it is expected that $R_{xtp} > R_i$ and $Sag_{fit} > Sag_{sub}$. This was always in our recordings with R_{xtp} and Sag_{fit} typically being around 25–30% larger.

We also measured the size of the rebound potential (V_{rbd}) seen when negative current injection was ceased. This was measured as the difference between V_{bsl} and the most depolarized potential observed following removal of current injection V_{posmax}. As expected, V_{rebd} was strongly positively correlated with both Sag_{fit} and Sag_{sub}.

Action potential threshold was defined as the voltage at the foot of the action potential where dV/dt first exceeds 15 V s^{-1}. Action potential width was measured at −15 mV, a membrane potential which lies approximately half way between action potential threshold (circa −60 mV) and action potential zenith (circa +30 mV) in CA1-PCs.

2.4. Western blotting

In the process of preparing tissue for electrophysiological recording single hippocampal slices were set aside from 11 PDAPP and 11 WT littermate controls. Immediately following their preparation the slices were snap frozen with liquid nitrogen, they were then thawed and homogenized in RIPA lysis buffer (Sigma, UK) containing both phosphatase inhibitor 2 + 3 (Sigma, UK) and protease inhibitor cocktail (Roche, UK). Following this the lysate was again snap frozen and stored at −80 °C until used with other samples in blotting.

For Western blotting first the protein content of each sample was determined using the bicinchoninic acid assay (BCA), (Sigma, UK). Protein (15 μg) was then separated on 4–20% graded SDS-PAGE gels and transferred onto PVDF membrane (BioRad, UK). Membranes were incubated with the 4G8 mouse monoclonal antibody raised against Amyloid-β (1:1000 dilution, Millipore, UK), followed by incubation with peroxidase-conjugated goat antibody to mouse IgG (Sigma, UK). The blots were then developed with enhanced chemiluminescence (ECL) reagent (Pierce, Biotechnology, Rockford, USA). The same samples were stripped and re-probed for β-actin (Abcam, Cambridge, UK) which acted as a loading control. Optical densities of immunoreactive bands were quantified using NIH ImageJ software (downloaded from http://rsb.info.nih.gov/ij/). Aβ immunoreactivities were normalized to the quantity of total β-Actin band intensity in each lane.

2.5. Data presentation

All data are presented as mean ± SEM. Each data point represents a recording from a single CA1 pyramidal neurone. In total over 30 mice of each genotype were used in this study. In the box plots shown in Figs. 2, 3 and 6, the individual symbols to the left plot data from every individual recording whereas the boxes to the right show the upper and lower standard error and the median (boxes), plus the mean (central symbol). Following testing for normality comparisons between groups were made using Student's *t*-test or ANOVA as appropriate.

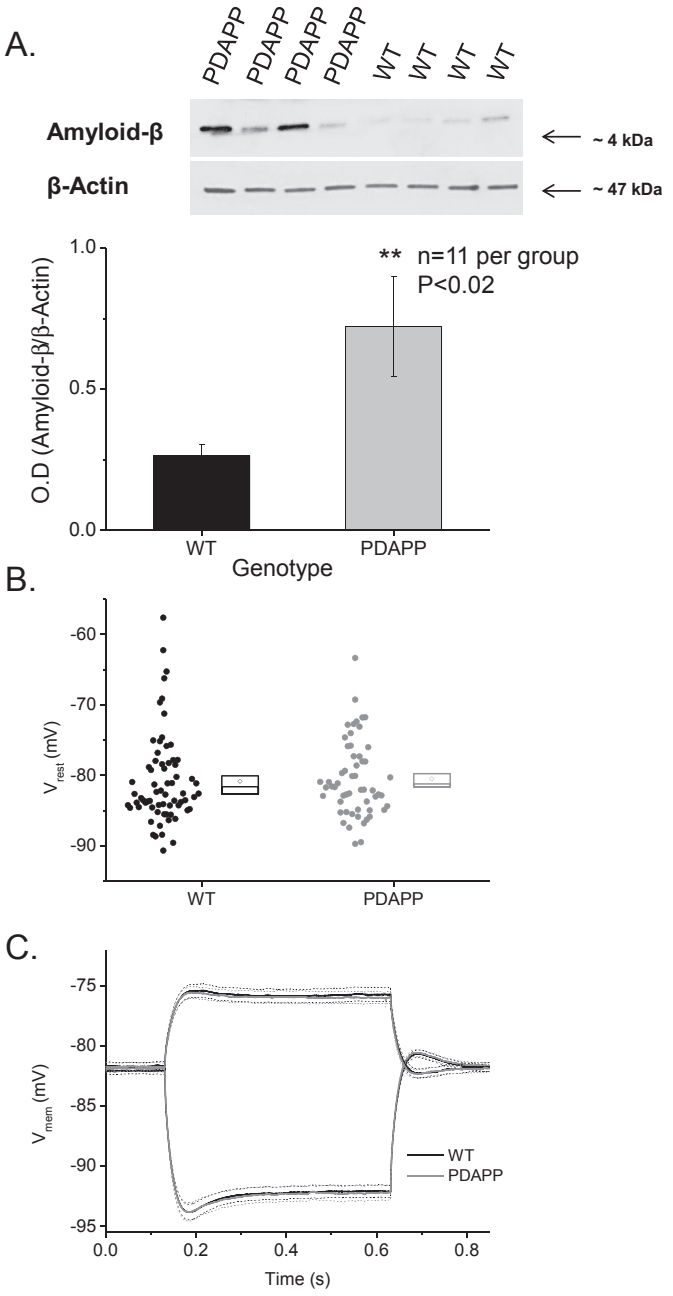

Fig. 2. Comparison of resting potential and voltage responses to subthreshold current injections. A) Top, an example Western blot presenting data from 4 PDAPP and 4 WT mice. Data for both Aβ and the housekeeping protein actin are shown. Bottom, pooled Western blot data from 11 animals of each genotype plotting the ratio of the Aβ signal to that derived from actin. The groups were significantly different when compared with an unpaired *t*-test. B) A graph comparing the zero current potential recording soon after gaining whole cell access (V_{rest}) for CA1-PC of WT and PDAPP mice. In these and all subsequent plots of this type each symbol represents a single recording whereas the boxes adjacent to the right present group data for mean (central diamond) as well as median and standard error (box). In this and all other figures WT data are in black and PDAPP data in grey. C) Average membrane voltage responses to −100 pA (downward) and +50 pA (upward) current injections lasting 500 ms and applied to cells at ~−82 mV. The dashed lines are standard error of the mean. Data from WT (black) and PDAPP (grey) mice are almost indistinguishable.

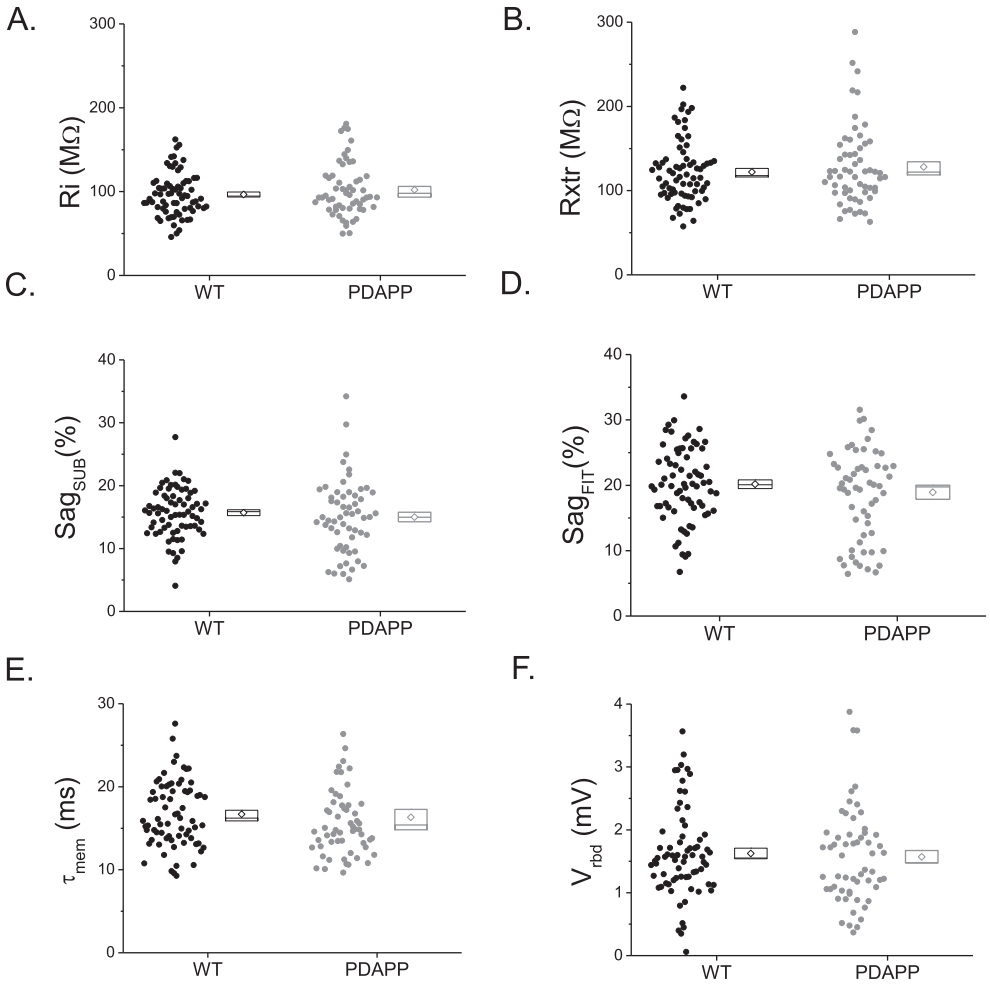

Fig. 3. Comparisons of multiple subthreshold intrinsic properties between WT and PDAPP littermates. The graphs present comparisons of multiple intrinsic properties measured from the voltage response to a −100 pA current stimulus. Data are shown for resting input resistance measured two ways, R_i (A), R_{xtr} (B); sag measured two ways, Sag_{sub} (C) and Sag_{fit} (D), τ_{mem} (E) and V_{rbd} (F). For details on calculation of these parameters see Methods and Fig. 1.

3. Results

The original descriptions of the PDAPP mouse demonstrated the presence of an amyloid plaque pathology as early as 6 months (Games et al., 1995), the extent of this pathology then grew in severity as the animals aged. In the PDAPP cohorts we have studied, however, the development of plaque pathology is less aggressive, and at the timepoint studied here there were essentially no visible plaques. Abeta levels were however significantly elevated as demonstrated by Western blotting analysis of 11 PDAPP and 11 WT littermate mice (Fig. 2A).

Others have reported resting potentials of some neurones to be depolarized in the face of an amyloid pathology (Minkeviciene et al., 2009; Verret et al., 2012). In this study the zero current potential measured in current clamp soon after obtaining whole cell access was not different between the two genotypes (−80.8 ± 0.8 mV, $n = 68$ in WT animals and −80.5 ± 0.7, $n = 56$ in PDAPPs, Fig. 2B, Table 1). Thus, as found in our previous study of PSAPP mice (Brown et al., 2011), under our recording conditions the resting potential of CA1-PCs does not seem to be perturbed by elevated Aβ.

Although resting potentials were not different across the two genotypes there was the expected spread of values between cells (illustrated by the symbols in Fig. 2B). Most intrinsic properties of neurones (with the exception of capacitance) exhibit some dependence on membrane potential, for example the input resistance of pyramidal cells varies with membrane potential, largely due to the presence of HCN and Kv7 channels. Thus, to reduce cell-to-cell variability in intrinsic parameters arising from resting potential variance, the remainder of our characterizations were made from a membrane potential set to approx −82 mV by application of the required small amount current injection. In post-hoc analysis of the recordings the actual membrane potentials achieved by this manipulation averaged −82.0 ± 0.3 mV, $n = 71$

Table 1
Intrinsic parameters and action potential waveform in WT and PDAPP mice. NS = not significantly different.

	WT	PDAPP	
V_{rest} (mV)	−80.8 ± 0.8	−80.5 ± 0.7 mV	NS
V_{maxneg} (mV)	−11.5 ± 3.2	−12.1 ± 3.8 mV	NS
V_{rbd} (mV)	1.6 ± 0.7	1.6 ± 0.8 mV	NS
R_{in} (MΩ)	96.6 ± 25.5	102.1 ± 31.7 mΩ	NS
R_{xtp} (MΩ)	122.1 ± 36.1	128.2 ± 46.8 mΩ	NS
τ_{mem} (ms)	16.7 ± 4.0	16.3 ± 7.2 ms	NS
Sag_{sub} (%)	15.7 ± 3.9	15.0 ± 5.8	NS
Sag_{fit} (%)	20.2 ± 5.7	18.9 ± 8.2	NS
AP peak (mV)	26.9 ± 7.4	25.6 ± 7.2	NS
AP max. rate of rise (mV ms^{-1})	451.7 ± 80.5	468.2 ± 93.4	NS
AP width at −15 mV (mV)	0.7 ± 0.1	0.6 ± 0.1	$p < 0.001$
AP threshold (mV)	−59.6 ± 4.1	−60.6 ± 3.4	NS

and −82.1 ± 0.1 mV, n = 58, for the WT and PDAPP groups, respectively.

A 500 ms injection of 100 pA of negative current into CA1-PCs of both genotypes caused a classical response of membrane charging towards a negative peak followed by "sag" back to a somewhat less negative steady state membrane potential. Following cessation of the applied negative current, the membrane potential depolarized again and overshot its resting level to produce a transient rebound potential which decayed back to rest over around 200 ms. Fig. 2C plots the average of these voltage responses from all 71 WT and 58 PDAPP cells examined in this way; it is clearly apparent that they are very similar. In agreement with this, the average responses to a 50 pA depolarizing current injection were also very similar (Fig. 2C). To confirm this similarity statistically, we quantified on a cell-by-cell basis, the membrane time constant (τ_{mem}), the maximum hyperpolarization achieved (V_{maxneg}), the input resistance (measured in two different ways, R_i and R_{xtp}, see Methods) the amount of sag (measured in two different ways, Sag_{sub} and Sag_{fit} see Methods) as well as the amplitude of the rebound potential (V_{rbd}) following cessation of current injection. This analysis was performed on the responses to −100 pA current injections. As shown in Fig. 3A–F and Table 1, none of these parameters were significantly different when the two genotypes were compared.

We tested action potential firing responses to current stimuli ranging from +50 to +300 pA in applied in 50 pA increments (Fig. 4A). This was also performed using the same set pre-stimulus membrane potential of −82 mV. When given a sufficiently large stimulus every cell of both genotypes produced action potential firing. The fraction of the total population of each genotype firing one or more spikes for each amplitude of current stimulus is shown in Fig. 4B. This suggests that cells in PDAPP mice are slightly easier to produce action potential firing in when using weak current stimuli, for example 46% of WT CA1-PC fired in response to +100 pA whereas 57% fired in PDAPP mice, however this was not a significant difference (2-sample K–S test). Fig. 4C and D plot the mean number of spikes fired for each magnitude of current stimulus. The data in Fig. 4C are average spike counts for all cells including those not firing (i.e. a spike count of zero) for a given stimulus. Whereas in Fig. 4D, data are shown only for cells that fired at least one spike in response to the corresponding stimulus amplitude. In either situation, although significantly more spikes were fired as the stimulus current was increased, there was no difference in spike number between the two groups.

For each depolarizing stimulus applied, as well as analysing the number of CA1-PC firing, or the number of spikes fired, it is also important to investigate the temporal pattern of spiking. This is exemplified by our previous study of PSAPP mice in which although fewer spikes fired in total, they fired in a more bursty manner, exhibiting a period of higher frequency firing close to the onset of the current stimulus, particularly with weak current injections (Brown et al., 2011); relating to this increase propensity to fire at high frequencies, CA1-PC also exhibited a larger spike after depolarization when activated with a short (2 ms) strong (2 nA) current injection (Brown et al., 2011). In the present study, broadly similar observations were made as illustrated by the plots of instantaneous frequency versus spike pair number for each of the first 10 inter-spike intervals (Fig. 5A–E). Data are shown for current injections ranging from +100 to +300 pA applied to both genotypes (50 pA depolarizing stimuli only produced spikes in 2 of 73 WT and 3 of 58 PDAPP neurones). These graphs show that, as is classically reported in CA1-PC, the first action potentials to fire arise at higher frequencies (e.g. 180 Hz for 300 pA stimuli), before spike frequency accommodation develops and reduces the mean firing rate to somewhere between 25 and 50 Hz. Also apparent is that the firing frequency was consistently higher in PDAPP cells, an effect that is particularly marked for the weaker (and perhaps more physiologically pertinent) current stimuli. In line with this, the amplitude of the fast ADP that followed a single action potential triggered by a 2 ms, 2 nA current stimulus was significantly larger in PDAPP mice (Fig. 5F). In contrast, the small AHP that follows the ADP evoked in this fashion was not altered in size ($P > 0.5$).

In our published study of PSAPP mice we also identified changes in action potential waveform. Specifically, we observed a decreased action potential height, rate of rise and width at −15 mV, whereas action potential threshold was unaltered (Brown et al., 2011). Here, as in our PSAPP study, we analysed the waveform of the first spike fired by a 300 pA current stimulus applied at −82 mV (Fig. 6A–D). Compared to WT littermates, in PDAPP animals we did not see any significant change in spike height or rate of rise, however, we saw a significant decrease in spike width similar to that we previously identified in PSAPP mice (Brown et al., 2011). Also as in PSAPP mice, we did not see any change in action potential threshold. The narrower action potential but lack of change in other parameters is further illustrated in Fig. 7 which plots the peak-aligned average spike waveforms from all of our PDAPP and WT recordings of CA1-PC.

4. Discussion

In this study we have used brain slice patch clamp methods to investigate the intrinsic excitability properties of the Aβ-overproducing PDAPP mouse. This is a well established model of CNS amyloidopathy produced by transgenic expression of a known disease-causing mutation in amyloid precursor protein (Games et al., 1995). To our knowledge, a study of intrinsic excitability properties in neurones of this model has not been performed elsewhere. This investigation was specifically designed to closely mirror our previous work in different Aβ overproducing mice, Table 2 summarizes and compares the finds of this study and our other recently published work on PSAPP mice (Brown et al., 2011). This may suggest to some that the present study is not especially novel or interesting, just a repeat of previous work in a different model. We feel, however, for any class of pathological model it is important to establish which neurophysiological changes are consistently observed in multiple mouse lines, because this will instil greater confidence that these outcomes represent pathology-dependent, rather than single model-dependent, phenotypes.

In this respect, one might argue that no reliable single neurophysiological outcome is known to reliably occur in multiple Aβ overproducing mice lines. Probably the most widely studied neurophysiological phenotypic measure in such mice is the extent of NMDA receptor-dependent hippocampal long-term potentiation. This has been the subject of dozens of historical studies performed in either the Schaffer collateral commissural or perforant pathways both in vitro and vivo (reviewed in Randall et al. (2010)). More recently this literature has been supplemented by the first investigations of NMDA receptor-independent LTP in mossy fibres (Witton et al., 2010). Although some studies find LTP to be depressed by amyloidopathy, this it is far from a universal observation, with many reports of unaltered LTP in animals despite the presence of an advanced plaque pathology. There is even one report of enhanced LTP in animals with quite advanced pathology (Jolas et al., 2002). Thus, it appears there may be a need for a more universal or reliable functional outcome that can both be used to help understand the disease process and to aid in the development of disease modifying therapies.

4.1. Resting potential

Although others have reported changes to neuronal resting potentials in transgenic mice that overproduce Aβ (Minkeviciene

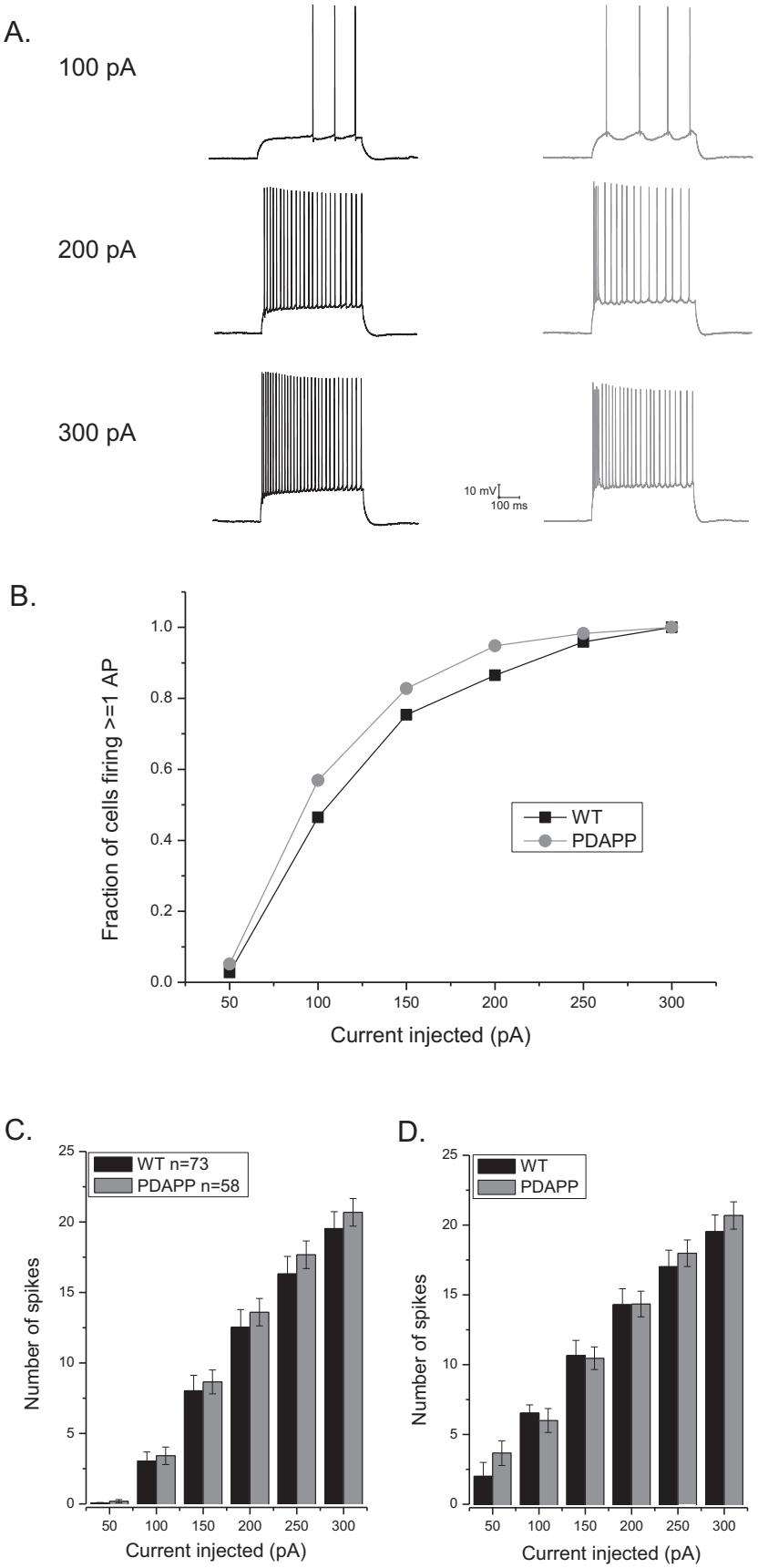

Fig. 4. Current thresholds and action potential counts in WT and PDAPP mice. A) Example recordings of voltage responses to 500 ms injections of 100, 200 or 300 pA of positive (i.e. depolarizing) current. The cell on the left was from a WT animal and that on the right from a PDAPP mouse. B) A graph plotting the fraction of all cells tested that produced at least one action potential in response to a given level of current injection. Although in PDAPP mice a larger proportion of cells fired for each level of stimulus (except 300 pA where all

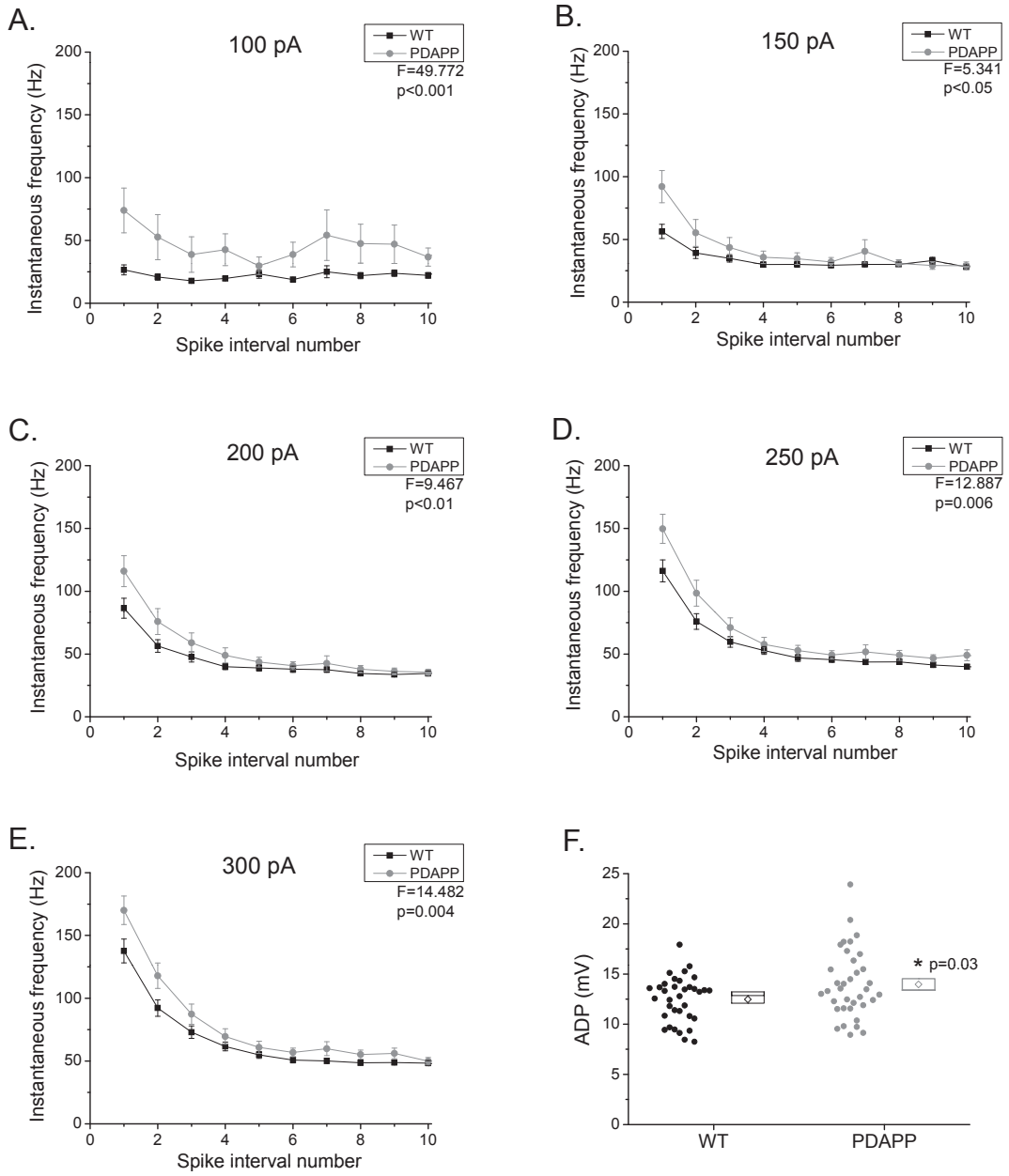

Fig. 5. Higher frequency firing is seen in PDAPP mice A–E) Graphs plotting, for current injections of 100–300 pA, the mean instantaneous firing rate of WT and PDAPP CA1-PC for each of the first 10 interspike intervals produced. Thus, the first spike interval is between the first and second spike, the second spike interval between the 2nd and 3rd spike etc. Although for most stimuli the firing rates become quite similar after a few action potentials have fired the initial firing rates are always higher in the PDAPP animals. F) A graph of the amplitude of the fast ADP observed following a 2 ms duration, 2 nA current injection.

et al., 2009) (Verret et al., 2012), we did not find this to be the case in CA1-PCs of PDAPP mice (Fig. 2B). This lack of change is in agreement with our previously published study of 8–9 month old PSAPP mice (WT: −78.0 ± 0.7 mV, n = 22 versus PSAPP: −78.8 ± 1.2, n = 22, Brown et al., 2011) and work in pre-plaque CRND8 mice (Wykes et al., 2012). We have also not seen a change in resting potential of CA1-PC when studying 15 month old PSAPP mice (WT −78.2 ± 1.0 mV (n = 25) versus PSAPP −79.4 ± 1.2 mV (n = 18), Claire Booth, AR and JB, unpublished observations) and 2 month old PSAPP mice (Brown et al., 2011). Furthermore, in other unpublished studies from our lab employing very similar recording conditions, we have also not seen changes to resting potential of CA1-PCs in the widely studied Tg2576 mouse line. Indeed, this was the case in both 2 year old, amyloid plaque-bearing, Tg2576 mice (WT: −76.8 ± 1 mV, n = 23 versus Tg2576: −76.1 ± 0.8 mV, n = 23) or 8 month old Tg2576 mice (WT: −77.1 ± 1.0 mV, n = 13 versus Tg2576: −75.3 ± 1.0 mV, n = 13). At this latter age there is not a significant amyloid plaque pathology but soluble Aβ is elevated and

cells fired in both groups), there was not a significant difference between the groups (2-sample K–S test). C) A histogram presenting the mean number of spikes fired for each level of depolarizing stimulus including sweeps in which no spikes fired. D) The same dataset as in (C) but presenting the number of spikes fired only for sweeps in which one of more spikes fired.

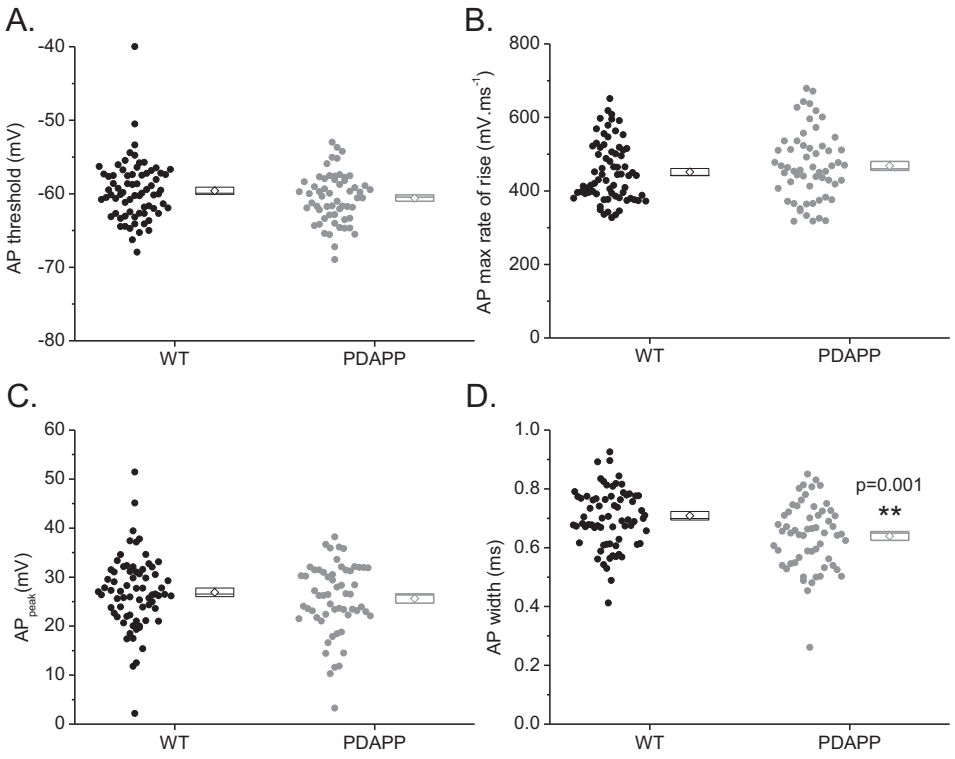

Fig. 6. Narrower action potentials are observed in CA1-PC of PDAPP mice. Scatter and box plots of four key action potential waveform parameters namely threshold (A), maximum rate of rise (B), peak amplitude of depolarization (C) and width at −15 mV (D). All data are from the first action potential produced by a 300 pA current stimulus. Only the width was different between the groups with narrower spikes seen in the CA1-PC of PDAPP mice.

Aβ-related functional deficits have been reported (Jacobsen et al., 2006). As well as a lack of change of resting potential in CA1-PC of PDAPP mice, we have also not seen any change to the resting potential of GABAergic interneurones in stratum oriens of these animals in recordings made under very similar conditions (WT −68.7 ± 0.9, $n = 73$ versus PDAPP: −68.3 ± 1.4, $n = 48$, Franceso Tamagnini, AR and JB unpublished observations).

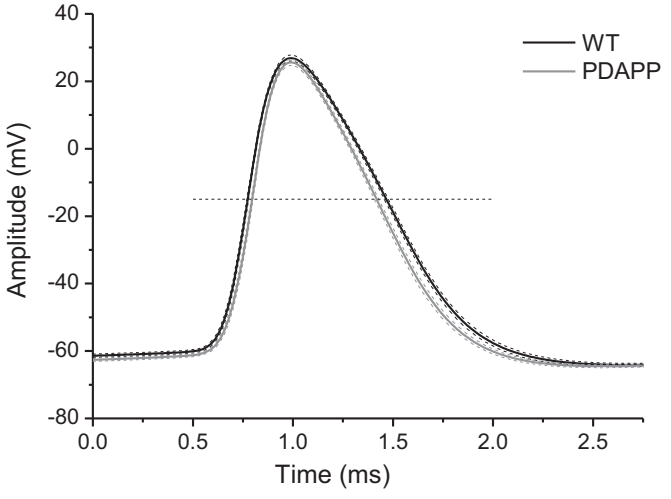

Fig. 7. Average action potential waveforms confirm narrower spikes in PDAPP mice. A plot illustrating the average action potential waveforms from the PDAPP and WT groups. To create the plot spikes were temporally aligned by their peaks prior to averaging, 1 ms of data was taken before the peak and 1.75 ms afterwards. The thin dashed lines either side of the action potential trajectory reflect standard errors. The horizontal dashed line is at −15 mV the voltage at which action potential width was measured in Fig. 6 and Table 1. Note the action potential width is equally different at other potentials.

4.2. Other subthreshold intrinsic properties

Changes to resting input resistance, membrane time constant, or sag can make significant alterations to the intrinsic excitability and electrical dynamics of neurones. For example, changes to resting input resistance will modify how just about all current stimuli affect a cell's response. Consequently, we have been mindful to study these parameters carefully. Thus, we measure input resistance not only from the post-sag, steady-state, voltage response to a hyperpolarizing current injection (which incorporates the

Table 2
A comparison of alterations to a range of intrinsic properties seen in this study and our previous investigation of PSAPP mice at 8–10 months.

	PDAPP	PSAPP
V_{rest}	NC	NC
V_{maxneg}	NC	NC
V_{rbd}	NC	Decreased
R_{in}	NC	NC
R_{xtp}	NC	NC
τ_{mem}	NC	NC
Sag_{sub}	NC	Decreased
Sag_{fit}	NC	Decreased
Number of spikes in 500 ms	NC	Decreased
Spike frequency	Increased	Increased
ADP amplitude	Increased	Increased
AP-peak	NC	Decreased
AP max rate of rise	NC	Decreased
AP width at −15 mV	Narrower	Narrower
AP threshold	NC	NC

additional activation of I_h that occurs), but also make a measurement from the infinite time extrapolation of the exponential fit to the membrane charging curve. We also employ the same fit to generate a second determination of the level of sag over and above that determined simply from the observed negative peak and post-sag, steady-state negative deflection. Furthermore, because input resistance, membrane time constant and sag are known to have a dependence on membrane voltage, we usually measure them using a hyperpolarizing current injection applied at a set pre-stimulus membrane potential of −82 mV.

With these approaches we failed to identify any differences in input resistance, membrane time constant or sag between PDAPP and WT mice (Fig. 3). Furthermore, the estimate of the capacitance derived by dividing the membrane time constant by the resting input resistance (derived from the fit to membrane charging) was not different between the two genotypes (WT: 147 ± 6 pF versus 138 ± 7 pF, $P = 0.33$), indicating there was not a major change in neuronal surface area.

The unaltered input resistance of PDAPP mice is in agreement with our previous work on PSAPP neurones at 2 and 8 months (Brown et al., 2011) and is also what is found in these animals at 15 months (Claire Booth, AR and JB, unpublished observations). In contrast, we have found input resistance to be circa 30% lower in 2 year old Tg2576 mice ($n = 20$) compared to WT littermates ($n = 17$), a significant difference ($P < 0.005$, JB and AR unpublished observations).

The almost identical levels of sag we observed in PDAPP and WT mice stands in contrast to our recordings from PSAPP mice under very similar conditions, where we found the Aβ overproducing line exhibited a significant, ~30%, decrease in the extent of hyperpolarization-triggered sag compared to WT littermates. This decrease was observed with both methods for measuring sag, and was also seen when the hyperpolarizing current stimulus was either −50 or −100 pA (AR and JB, unpublished observations). In Tg2576 mice we have also observed a significant decrease in sag of around 25% at 24 months of age – although whether this is solely due to consequences of the change in input resistance that arises (see above) is not presently clear. Interestingly in the rTg4510 transgenic mouse model of tauopathy, we have observed a significant increase in sag in multiple classes of neurone, including CA1-PC (Claire Booth, AR and JB, manuscript in preparation).

4.3. Changes to suprathreshold behaviours

Although we were unable to detect any changes to basic, subthreshold intrinsic properties in PDAPP mice, significant effects of genotype became apparent when we used suprathreshold current pulses to depolarize CA1-PC beyond action potential threshold. One clear observation was that these pyramidal cells fired faster in the Aβ-overproducing mice. This was apparent at all levels of current stimulus, and particularly striking for weaker current injections. This is, for the most part, a similar observation to our findings in PSAPP mice, however, in these animals the differences between genotypes disappeared with the very strongest depolarizing current stimuli. As we and others have described previously, the ionic conductances that produce the fast ADP in hippocampal pyramidal cells are particularly important in determining bursty/high frequency firing responses to depolarizing stimuli (Brown and Randall, 2009). When we measured the size of this afterpotential using our standard approach it was found to be larger (Fig. 5F), similar to our observations in PSAPP mice (Brown et al., 2011). Overall these finding indicate that CA1-PC exhibit an intrinsic hyperexcitability, something we have proposed may contribute to the regional network hyperexcitability that arises in Aβ overproducing mice, and may also be a facet of AD in humans (Brown et al., 2011; Palop and Mucke, 2009; Verret et al., 2012).

We also examined action potential waveforms in PDAPP mice as we had found these to be modified in multiple ways in PSAPP animals. Although we did not find any evidence for the changes to peak or rate of rise of action potentials comparable to those identified in PSAPP mice (Brown et al., 2011), we did see a very similar degree of spike narrowing in both studies. Indeed the data from the two studies are nearly identical. Thus, spike widths at −15 mV of around 0.7 ms were seen in WT neurones (0.70 ± 0.01 ms ($n = 24$, PSAPP study) and 0.71 ± 0.01 ($n = 71$, this study)), whereas spike widths were closer to 0.6 ms in the transgenic mice (0.62 ± 0.1 ($n = 21$, PSAPP mice) and 0.64 ± 0.1 ms ($n = 58$, PDAPP mice)). The lack of change to action potential height and rate of rise in PDAPP mice suggests these animals may not have developed the prominent Na^+ channel deficit we identified in PSAPP mice (Brown et al., 2011). It also indicates that the change in spike width seen in both studies does not require alterations to spike height or rate of rise to develop.

In unpublished studies from our laboratory we found that the significantly decreased spike width in 8–9 Mo PSAPP mice persisted at 15 months of age. We have also observed that in 2 year old Tg2576 mice a very similar ~12% reduction in spike width is seen under similar experimental conditions (0.67 ± 0.02 ms (WT, $n = 17$) versus 0.60 ± 0.03 ms (Tg2576, $n = 20$)), although this change just failed to reach statistical significance ($P < 0.06$), probably due to the lower statistical power is this study than in our work on cohorts of PSAPP and PDAPP. In a different laboratory using quite similar methods, a significant, age-dependent, decrease in action potential width of CA1-PC has also been reported CRND8 mice at a pre-plaque stage (Wykes et al., 2012). CRND8 is an alternative Aβ-overproducing mouse line based on a doubly mutated form of APP harbouring both the Swedish and Indiana mutations. Thus based on three mice lines we have studied and one study performed elsewhere (Wykes et al., 2012), it would seem that a 10–15% narrowing of spikes in CA1-PC of Aβ overproducing transgenic mice is a repeatable finding across multiple transgenic lines; although investigation of an even greater number of Aβ-overproducing lines would be useful to confirm the generality of this finding.

The changes to action potential width may appear modest, averaging between 10 and 15%, however, this is sufficient to produce substantial downstream effects on activation of other processes. For example, because of the nature of the gating kinetics of voltage-sensitive Ca^{2+} channels the narrower action potentials in PSAPP or PDAPP mice will produce around 40% less Ca^{2+} entry per spike, something we have demonstrated both experimentally with patch clamp recording and with mathematical modelling (unpublished observations). In CA1-PC of CRND8 mice a reduced Ca^{2+} entry per spike has also been demonstrated with multiphoton imaging in brain slices (Wykes et al., 2012). Given the profound role of Ca^{2+} in multiple key cellular signalling pathways, this change in Ca^{2+} entry per spike could alone lead to multifaceted functional consequences of altered action potential width associated with amyloidopathy. One potential area very worthy of examination would be the gating of presynaptic Ca^{2+} channels mediating neurotransmitter release. Although this would also require understanding if the changes to action potential waveform we and others observe at the neuronal cell body also occur along the axonal arbour and within the presynaptic bouton.

It is interesting to speculate that the reduction in action potential width we see in transgenic mice reflects a homeostatic rebalancing mechanism to counter the intrinsic hyperexcitability that generates higher frequency, more bursty firing patterns (Fig. 4). Alternatively the converse may be the case, namely that the altered firing patterns are a homeostatic response to counteract the presence of a narrower action potential. Either way, understanding the cellular mechanisms responsible for the presence of narrower

spikes in Aβ-overproducing mice will be informative, and may also provide novel routes to addressing some of the circuit deficits that develop in the face of a persistent amyloidopathy. The most obvious source of narrower spikes would be enhanced functional contributions from fast gating potassium channels with roles in action potential repolarization. This could occur potentially through an increase in cell surface channel density or instead from an alteration to gating biophysics or even permeation properties. In a previous study increases in Kv3.1 have been proposed as a candidate mechanism (Wykes et al., 2012). Other mechanisms independent of K^+ channels are also feasible, for example a loss of a contribution to the action potential waveform from voltage-gated Ca^{2+} channels or faster Na^+ channel inactivation could both contribute to a narrowing of action potential waveform.

In summary this work both adds to, and complements, previous studies of intrinsic excitability in transgenic mice that overproduce Aβ peptides. By employing methods very similar to those used in our own previous investigation we have identified potentially common outcomes that may occur in multiple, and perhaps all Aβ-overproducing mouse lines. In the near future we are embarking on similar studies of CA1-PC in 2 additional transgenic mouse lines which express a robust amyloidopathy. We feel that only by going to these lengths will we discover the most robust and perhaps significant neurophysiological changes associated with this form of pathology.

References

Brown, J.T., Chin, J., Leiser, S.C., Pangalos, M.N., Randall, A.D., 2011. Altered intrinsic neuronal excitability and reduced Na^+ currents in a mouse model of Alzheimer's disease. Neurobiol. Aging 32, 2109.e1–2109.e14.

Brown, J.T., Randall, A.D., 2009. Activity-dependent depression of the spike after-depolarization generates long-lasting intrinsic plasticity in hippocampal CA3 pyramidal neurons. J. Physiol. 587, 1265–1281.

Brown, J.T., Richardson, J.C., Collingridge, G.L., Randall, A.D., Davies, C.H., 2005. Synaptic transmission and synchronous activity is disrupted in hippocampal slices taken from aged TAS10 mice. Hippocampus 15, 110–117.

Chapman, P.F., White, G.L., Jones, M.W., Cooper-Blacketer, D., Marshall, V.J., Irizarry, M., Younkin, L., Good, M.A., Bliss, T.V., Hyman, B.T., Younkin, S.G., Hsiao, K.K., 1999. Impaired synaptic plasticity and learning in aged amyloid precursor protein transgenic mice. Nat. Neurosci. 2, 271–276.

Driver, J.E., Racca, C., Cunningham, M.O., Towers, S.K., Davies, C.H., Whittington, M.A., LeBeau, F.E., 2007. Impairment of hippocampal gamma-frequency oscillations in vitro in mice overexpressing human amyloid precursor protein (APP). Eur. J. Neurosci. 26, 1280–1288.

Fitzjohn, S.M., Doherty, A.J., Collingridge, G.L., 2008. The use of the hippocampal slice preparation in the study of Alzheimer's disease. Eur. J. Pharmacol. 585, 50–59.

Games, D., Adams, D., Alessandrini, R., Barbour, R., Berthelette, P., Blackwell, C., Carr, T., Clemens, J., Donaldson, T., Gillespie, F., et al., 1995. Alzheimer-type neuropathology in transgenic mice overexpressing V717F beta-amyloid precursor protein. Nature 373, 523–527.

Hardy, J., 2009. The amyloid hypothesis for Alzheimer's disease: a critical reappraisal. J. Neurochem. 110, 1129–1134.

Hsia, A.Y., Masliah, E., McConlogue, L., Yu, G.Q., Tatsuno, G., Hu, K., Kholodenko, D., Malenka, R.C., Nicoll, R.A., Mucke, L., 1999. Plaque-independent disruption of neural circuits in Alzheimer's disease mouse models. Proc. Natl. Acad. Sci. U. S. A. 96, 3228–3233.

Jacobsen, J.S., Wu, C.C., Redwine, J.M., Comery, T.A., Arias, R., Bowlby, M., Martone, R., Morrison, J.H., Pangalos, M.N., Reinhart, P.H., Bloom, F.E., 2006. Early-onset behavioral and synaptic deficits in a mouse model of Alzheimer's disease. Proc. Natl. Acad. Sci. U. S. A. 103, 5161–5166.

Jolas, T., Zhang, X.S., Zhang, Q., Wong, G., Del Vecchio, R., Gold, L., Priestley, T., 2002. Long-term potentiation is increased in the CA1 area of the hippocampus of APP(swe/ind) CRND8 mice. Neurobiol. Dis. 11, 394–409.

Lalonde, R., Fukuchi, K., Strazielle, C., 2012. APP transgenic mice for modelling behavioural and psychological symptoms of dementia (BPSD). Neurosci. Biobehav. Rev. 36, 1357–1375.

Larson, J., Lynch, G., Games, D., Seubert, P., 1999. Alterations in synaptic transmission and long-term potentiation in hippocampal slices from young and aged PDAPP mice. Brain Res. 840, 23–35.

McGowan, E., Sanders, S., Iwatsubo, T., Takeuchi, A., Saido, T., Zehr, C., Yu, X., Uljon, S., Wang, R., Mann, D., Dickson, D., Duff, K., 1999. Amyloid phenotype characterization of transgenic mice overexpressing both mutant amyloid precursor protein and mutant presenilin 1 transgenes. Neurobiol. Dis. 6, 231–244.

Minkeviciene, R., Rheims, S., Dobszay, M.B., Zilberter, M., Hartikainen, J., Fulop, L., Penke, B., Zilberter, Y., Harkany, T., Pitkanen, A., Tanila, H., 2009. Amyloid beta-induced neuronal hyperexcitability triggers progressive epilepsy. J. Neurosci. 29, 3453–3462.

Morrissette, D.A., Parachikova, A., Green, K.N., LaFerla, F.M., 2009. Relevance of transgenic mouse models to human Alzheimer disease. J. Biol. Chem. 284, 6033–6037.

Oddo, S., Caccamo, A., Shepherd, J.D., Murphy, M.P., Golde, T.E., Kayed, R., Metherate, R., Mattson, M.P., Akbari, Y., LaFerla, F.M., 2003. Triple-transgenic model of Alzheimer's disease with plaques and tangles: intracellular Abeta and synaptic dysfunction. Neuron 39, 409–421.

Palop, J.J., Chin, J., Roberson, E.D., Wang, J., Thwin, M.T., Bien-Ly, N., Yoo, J., Ho, K.O., Yu, G.Q., Kreitzer, A., Finkbeiner, S., Noebels, J.L., Mucke, L., 2007. Aberrant excitatory neuronal activity and compensatory remodeling of inhibitory hippocampal circuits in mouse models of Alzheimer's disease. Neuron 55, 697–711.

Palop, J.J., Mucke, L., 2009. Epilepsy and cognitive impairments in Alzheimer disease. Arch. Neurol. 66, 435–440.

Randall, A.D., Witton, J., Booth, C., Hynes-Allen, A., Brown, J.T., 2010. The functional neurophysiology of the amyloid precursor protein (APP) processing pathway. Neuropharmacology 59, 243–267.

Rocher, A.B., Kinson, M.S., Luebke, J.I., 2008. Significant structural but not physiological changes in cortical neurons of 12-month-old Tg2576 mice. Neurobiol. Dis. 32, 309–318.

Roder, S., Danober, L., Pozza, M.F., Lingenhoehl, K., Wiederhold, K.H., Olpe, H.R., 2003. Electrophysiological studies on the hippocampus and prefrontal cortex assessing the effects of amyloidosis in amyloid precursor protein 23 transgenic mice. Neuroscience 120, 705–720.

Spencer, J.P., Weil, A., Hill, K., Hussain, I., Richardson, J.C., Cusdin, F.S., Chen, Y.H., Randall, A.D., 2006. Transgenic mice over-expressing human beta-amyloid have functional nicotinic alpha 7 receptors. Neuroscience 137, 795–805.

Verret, L., Mann, E.O., Hang, G.B., Barth, A.M., Cobos, I., Ho, K., Devidze, N., Masliah, E., Kreitzer, A.C., Mody, I., Mucke, L., Palop, J.J., 2012. Inhibitory interneuron deficit links altered network activity and cognitive dysfunction in Alzheimer model. Cell 149, 708–721.

Witton, J., Brown, J.T., Jones, M.W., Randall, A.D., 2010. Altered synaptic plasticity in the mossy fibre pathway of transgenic mice expressing mutant amyloid precursor protein. Mol. Brain 3, 32.

Wykes, R., Kalmbach, A., Eliava, M., Waters, J., 2012. Changes in the physiology of CA1 hippocampal pyramidal neurons in preplaque CRND8 mice. Neurobiol. Aging 33, 1609–1623.

Zhang, H., Ma, Q., Zhang, Y.W., Xu, H., 2012. Proteolytic processing of Alzheimer's beta-amyloid precursor protein. J. Neurochem. 120 (Suppl. 1), 9–21.